



INVESTIGATION OF NOISE SOURCES IN A TWO-DIMENSIONAL MODEL AIRFRAME NOISE PROBLEM. PART 2: NOISE GENERATION MECHANISMS.

André V. G. Cavalieri

Instituto Tecnológico de Aeronáutica, Divisão de Engenharia Aeronáutica, Praça Mal. Eduardo Gomes, 50, Vila das Acácias
12228-900, São José dos Campos - SP, Brazil
andre@ita.br

William R. Wolf

Universidade Estadual de Campinas, Faculdade de Engenharia Mecânica, Departamento de Energia, Rua Mendeleev, 200, Unicamp
13083-970, Campinas - SP, Brazil
wolf@fem.unicamp.br

Abstract. *Direct numerical simulations (DNS) of a model airframe noise problem, consisting of a cylinder placed above a NACA 0012 airfoil at 5 deg. angle of incidence, are studied in order to assess the significance of dipole and quadrupole distributions in the radiated sound. It is seen that while the sound field for lower Mach number flows can be obtained accounting only for the dipole distribution on the solid surfaces, for $M_\infty = 0.5$ the quadrupole distribution is no longer negligible. To understand the differences caused by the compressibility effect, we perform a linear stability analysis of the cylinder wake, which is seen to have a wave-packet structure. The eigenfunctions so obtained are in close agreement with the DNS results, validating the application of the linear framework to the present problem. The linear stability analysis reveals that the Mach 0.5 flow comprises a wavepacket with higher spatial amplification, higher convective Mach number and a sudden downstream truncation, all of which are known to increase sound radiation, and explain the significant role of quadrupoles in the $M_\infty = 0.5$ configuration when compared to the $M_\infty = 0.3$ flow.*

Keywords: *aeroacoustics, airframe noise, wake instability*

1. INTRODUCTION

For subsonic Mach numbers, the numerical prediction of the radiated sound is often based on hybrid methods, with a direct computation of a turbulent flow and the subsequent calculation of the sound field using an acoustic analogy (a review of these techniques is given by Wang *et al.*, 2006). Lighthill's acoustic analogy (Lighthill, 1952) is often used due to its relative simplicity, with the formulation of Ffowcs Williams and Hawkings (1969) (FW-H) commonly used in airframe noise problems.

The analogy includes contributions from sources integrated along the geometry surfaces (monopoles and dipoles) as well as volumetric sources along boundary layer and wake regions (quadrupoles). Due to the cost of computing the volume integrals, quadrupole terms are often neglected. In low Mach number flows, this approximation should be reasonable since the effects of quadrupoles are small relative to the effects of dipoles and monopoles, but there is no theoretical Mach number limit for which the approximation is accurate; it may depend on the specific flow under study.

Recent studies have shown that, at moderate Mach numbers, quadrupole sources can have a non-negligible effect on far field acoustic predictions (Wolf and Lele, 2010, 2011). Additionally, it has been demonstrated that quadrupole sources have a significant impact on predictions involving airframe configurations, particularly those with wake interactions.

Related work by our group (Wolf *et al.*, 2013) showed a significant Mach number effect on the radiation of quadrupole sources of flows with interactions between cylinder and airfoil wakes. It is our purpose in the present paper to study the reasons for this Mach number effect, and evaluate under which circumstances quadrupole radiation may be relevant for airframe noise. We use the aeroacoustic predictions of a two-dimensional model airframe noise problem from Wolf *et al.* (2013) and evaluate if the fluctuations in the wakes can be described as a wavepacket resulting from a linear instability of the flow. Such description has proven useful in free jets (see Jordan and Colonius, 2013, for a review). Whenever appropriate, the wave-packet description of the source allows one to extract the flow features important for sound generation.

The paper is organised as follows. We describe the numerical methodology for the flow simulations and acoustic predictions in sections 2 and 3, respectively. A brief recapitulation of the results obtained for the flow and acoustic fields obtained by direct noise computation (DNC) is presented in section 4.1, and section 4.2 shows acoustic predictions obtained by DNC and the FW-H equation, with evaluations of the contributions of dipole and quadrupole sources to the total noise predictions. In section 5, we investigate how compressibility changes the hydrodynamic field and, consequently, the quadrupole radiation. First, we show in section 5.1 that the cylinder wake has a wave-packet structure. In section 5.2

linear stability is used to explain the properties of the wake wavepackets for different Mach numbers. Finally, in section 5.2.3 we summarize the trends obtained in the linear stability analysis, and relate them to quadrupole radiation.

2. FLOW SIMULATION

The general curvilinear form of the compressible Navier-Stokes equations is solved in conservation form. The numerical scheme for spatial discretization is a sixth-order accurate compact scheme (Nagarajan *et al.*, 2003) implemented on a staggered grid. The current numerical capability allows the use of overset grids with a fourth-order accurate Hermite interpolation between grid blocks (Bhaskaran and Lele, 2010). Compact finite-difference schemes are non-dissipative and numerical instabilities arising from insufficient grid resolution, mesh non-uniformities, approximate boundary conditions and interpolation at grid interfaces have to be filtered to preserve stability of the numerical schemes. The high wavenumber compact filter presented by Lele (1992) is applied to the computed solution at prescribed time intervals in order to control numerical instabilities. This filter is only applied in flow regions far away from solid boundaries. The time integration of the fluid equations is carried out by the fully implicit second-order scheme of Beam and Warming (1978) in the near-wall region in order to overcome the time step restriction. A third-order Runge-Kutta scheme is used for time advancement of the equations in flow regions far away from solid boundaries.

No-slip adiabatic wall boundary conditions are applied along the solid surfaces and characteristic plus sponge boundary conditions are applied in the far field locations. The sponge zones start 12 airfoil chords or 300 cylinder diameters downstream of the airfoil trailing edge, and should have negligible effect on the development of the two wakes discussed in the following sections, whose salient features are related to the first airfoil chord downstream of the trailing edge.

The numerical tool has been previously validated for several simulations of compressible flows involving sound generation and propagation (Wolf and Lele, 2010, 2011; Wolf *et al.*, 2012).

3. ACOUSTIC PREDICTIONS

The Ffowcs Williams and Hawkings (1969) (FW-H) acoustic analogy formulation is used to predict the acoustic field radiated by the unsteady flow simulations. The frequency domain FW-H equation in integral form is written as

$$\left[\hat{p}' H(f) \right] = - \int_{f=0} \left[i\omega \hat{Q}(\vec{y}) G(\vec{x}, \vec{y}) + \hat{F}_i(\vec{y}) \frac{\partial G(\vec{x}, \vec{y})}{\partial y_i} \right] dS - \int_{f>0} \hat{T}_{ij} H(f) \frac{\partial^2 G(\vec{x}, \vec{y})}{\partial y_i \partial y_j} dV, \quad (1)$$

where p' is the acoustic pressure, ω is the angular frequency, \vec{y} is a source location, \vec{x} is an observer location and the term $\hat{\cdot}$ represents a Fourier transformed quantity. The monopole and dipole source terms are

$$Q = [\rho(u_i + U_i) - \rho_0 U_i] \partial f / \partial x_i \quad (2)$$

and

$$F_i = [p \delta_{ij} - \tau_{ij} + \rho(u_i - U_i)(u_j + U_j) + \rho_0 U_i U_j] \partial f / \partial x_j, \quad (3)$$

respectively, and T_{ij} is the Lighthill stress tensor or quadrupole source term given by

$$T_{ij} = \rho u_i u_j + (p' - c_0^2 \rho') \delta_{ij} - \tau_{ij}. \quad (4)$$

Here, u_i is the fluid velocity vector, U_i is the FW-H surface velocity, p is the pressure, ρ_0 is the freestream density, ρ' stands for the acoustic density, c_0 is the speed of sound, δ_{ij} is the Kronecker delta and τ_{ij} is the viscous stress tensor. The term $f = 0$ represents the FW-H surface and $H(f)$ is the Heaviside function defined as $H(f) = 1$ for $f > 0$ and $H(f) = 0$ for $f < 0$. Source terms, observer locations and scattering bodies are assumed to be in steady uniform motion with $\vec{U} = (-U_1, 0)^t$. The convective Green's function is given by

$$G(\vec{x}, \vec{y}) = \frac{i}{4\sqrt{1-M^2}} e^{iM \frac{k}{(1-M^2)}(x_1-y_1)} H_0^{(2)} \left(\frac{k}{(1-M^2)} \sqrt{(x_1-y_1)^2 + (1-M^2)(x_2-y_2)^2} \right), \quad (5)$$

where M is the freestream Mach number defined as $M \equiv U_1/c_0$, k is the wavenumber and $H_0^{(2)}$ is the Hankel function of the second kind and order zero.

In the present work, the surface integrations appearing in Eq. (1) are computed along the scattering body surfaces. Therefore, $u_i = -U_i$ for the monopole and dipole source terms, which are then given by $Q = -\rho_0 U_i \partial f / \partial y_i$ and $F_i = [p \delta_{ij} + \rho_0 U_i U_j] \partial f / \partial y_j$, respectively. Furthermore, one can observe that the monopole source terms, Q , and the second component of the dipole source terms, $\rho_0 U_i U_j$, are steady in time and do not appear in the frequency domain formulation. The volume integrations in Eq. (1) are computed using a fast multipole method (FMM) (Wolf and Lele, 2010) that incorporates convective effects along a subset region of the flow field including the wake plus boundary layer

Table 1. Summary of flow configurations investigated. Configurations 5 and 6, highlighted in bold, are the focus of the present work.

| Configuration | Mach number | Position of cylinder center (x,y) |
|---------------|------------------|------------------------------------|
| 1 | $M_\infty = 0.1$ | (0.5c, 0.25c) half-chord |
| 2 | $M_\infty = 0.3$ | (0.5c, 0.25c) half-chord |
| 3 | $M_\infty = 0.5$ | (0.5c, 0.25c) half-chord |
| 4 | $M_\infty = 0.1$ | (1.0c, 0.25c) trailing edge |
| 5 | $M_\infty = 0.3$ | (1.0c, 0.25c) trailing edge |
| 6 | $M_\infty = 0.5$ | (1.0c, 0.25c) trailing edge |

regions, where the magnitude of quadrupole sources is non-negligible. Therefore, calculations of acoustic pressure can be performed by the following equation

$$\left[\hat{p}' H(f) \right] = \left\{ - \int_{f=0} \left[i\omega \hat{Q}(\vec{y}) G(\vec{x}, \vec{y}) + \hat{F}_i(\vec{y}) \frac{\partial G(\vec{x}, \vec{y})}{\partial y_i} \right] dS - \int_{f>0} \hat{T}_{ij} H(f) \frac{\partial^2 G(\vec{x}, \vec{y})}{\partial y_i \partial y_j} dV \right\}_{\text{FW-H}} + \quad (6)$$

$$\left\{ \frac{i}{4\pi\sqrt{1-M^2}} \left[\frac{1}{2\pi} \oint e^{i\vec{k} \cdot \vec{o}\vec{X}} e^{iMKX_1} L(\vec{o}, \vec{K}) d(\vec{K}/|\vec{K}|) + \sum_{n=-\varphi_{lv}}^{\varphi_{lv}} (-1)^n e^{iMKX_1} R^n(\vec{o}\vec{X}) L_{-n}(\vec{o}) \right] \right\}_{\text{FMM}}.$$

Details about the terms appearing in the equation above are given in [Wolf and Lele \(2010\)](#).

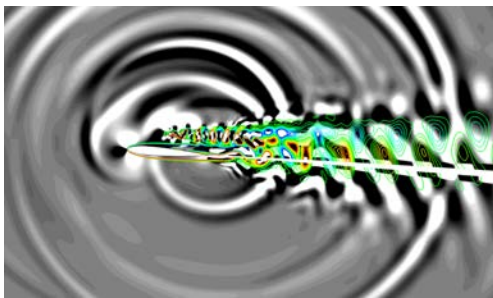
4. RESULTS

This section discusses results obtained by direct noise calculation (DNC) and the Ffowcs Williams-Hawkings (FW-H) equation for the unsteady flow past a cylinder in the proximity of a NACA 0012 airfoil. The flow configurations investigated allow a study of sound generation due to interaction of boundary layers and wakes, including vortex shedding. The flow Reynolds numbers based on the airfoil chord and cylinder diameter are $Re_c = 5000$ and $Re_d = 200$, respectively. The freestream Mach numbers considered in the flow calculations and acoustic predictions are $M_\infty = 0.1, 0.3$ and 0.5 , and the angle of incidence is fixed at $AoA = 5$ deg. The present grid configuration consists of body-fitted O-grid blocks around airfoil and cylinder surfaces and a background O-grid block that resolves the acoustic far field. The airfoil grid block is composed of 400×60 grid points, in the periodic and wall normal directions, respectively, and the cylinder grid block is composed of 240×50 grid points, in the periodic and wall normal directions. These grid blocks are designed to accurately resolve the laminar boundary layers that develop along the airfoil and cylinder surfaces. The far field background grid block has 400×625 points, in the periodic and wall normal directions, respectively, with smooth stretching to accurately capture the sound radiation. In order to evaluate the effects of cylinder position on acoustic scattering and diffraction, the cylinder grid block is displaced from the half-chord position to the trailing edge position. A summary of the flow configurations investigated is presented in Table 1. The airfoil has normalized chord $c = 1$ with trailing edge at $(x, y) = (1.0c, 0.0)$. Since the airfoil is at $AoA = 5$ deg, figures show the configuration rotated by -5 deg. All directivity plots in the paper are computed for a coordinate system located at the airfoil half-chord position.

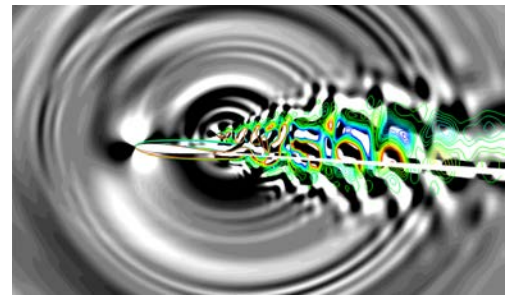
4.1 Flow and Acoustic Fields

Figures 1, 2 and 3 present snapshots of the flow and acoustic fields obtained by DNC for all configurations analyzed. Contours of z-component of vorticity along the airfoil and cylinder wake regions are shown in color and contours of dilatation are shown in grayscale. These figures allow a preliminary analysis of the effects of cylinder position and freestream Mach number on sound generation and propagation. In Figs. 1 (a) and (b), one can observe the presence of vortex shedding forming along the cylinder and airfoil wakes for both cylinder positions investigated for $M_\infty = 0.1$. For flow configurations with freestream Mach numbers $M_\infty = 0.3$ and $M_\infty = 0.5$, Figs. 2 and 3, respectively, different hydrodynamic features are observed due to a change in cylinder position. When the cylinder is placed at half-chord, the airfoil vortex shedding is suppressed due to wake interaction. One can also see that cylinder vortex shedding ceases further upstream as Mach number is increased. This effect is followed by wake stabilization and it can be observed in a comparison of Figs. 1 (a), 2 (a) and 3 (a). If the cylinder is placed at the trailing edge position, airfoil vortex shedding is developed for the entire range of Mach numbers analyzed. For all tested cases, one can notice that, further downstream along the wake, there is a merging of alternating vortical structures which characterizes a single vortex shedding frequency.

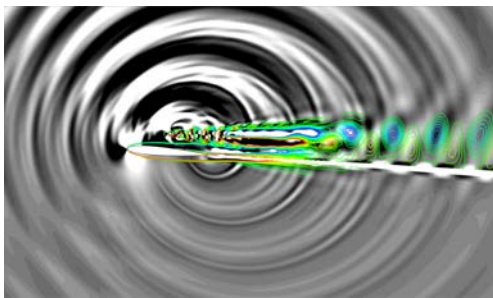
Far field sound radiation is also modified according to freestream Mach number and cylinder position. From Figs. 1, 2 and 3, it is clear that Mach number effects considerably modify the acoustic wavenumbers. Higher Mach numbers are



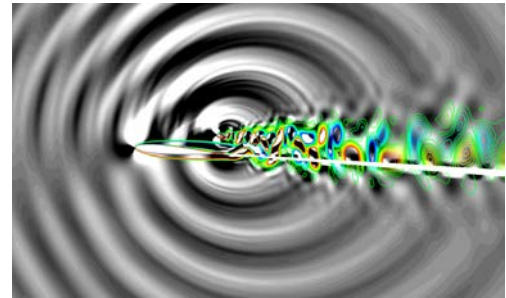
(a) Cylinder at half-chord position.



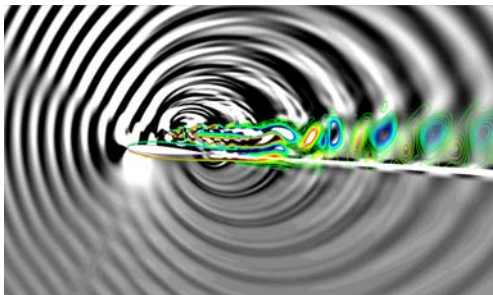
(b) Cylinder at trailing edge position.

Figure 1. Contours of z-vorticity in color and contours of dilatation in grayscale for $M_\infty = 0.1$.

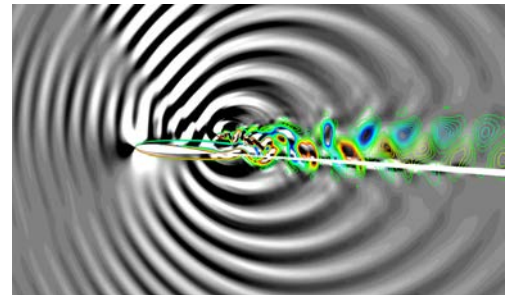
(a) Cylinder at half-chord position.



(b) Cylinder at trailing edge position.

Figure 2. Contours of z-vorticity in color and contours of dilatation in grayscale for $M_\infty = 0.3$.

(a) Cylinder at half-chord position.



(b) Cylinder at trailing edge position.

Figure 3. Contours of z-vorticity in color and contours of dilatation in grayscale for $M_\infty = 0.5$.

associated to higher frequencies with lower acoustic wavelengths. Doppler effects are also readily seen, specially in Fig. 3, for $M_\infty = 0.5$. Cylinder position impacts the scattering and diffraction characteristics of the acoustic field. In Figs. 1 (a), 2 (a) and 3 (a), it is possible to see the more pronounced reflection effects along airfoil surface and, in Figs. 1 (b), 2 (b) and 3 (b), one can observe that trailing edge diffraction effects are more prominent.

4.2 Noise Predictions

In Wolf *et al.* (2013), the quadrupole sources and their sound radiation were studied in detail. We review here some of those results for completeness, focusing on the cases we analyse in the present work, which correspond to configurations 5 and 6 on table 1.

In Fig. 4, field plots of the Reynolds stresses are shown for the cylinder vortex shedding frequency. In these figures, the cylinder is at the trailing edge position. In order to compare the spatial distribution of the separate Reynolds stress terms, $|\widehat{\rho u_i u_j}|$, for different Mach numbers, these noise sources are normalized by the maximum field values for each flow configuration. Without normalization, maximum values of longitudinal $|\widehat{\rho u_1 u_1}|$ and transversal $|\widehat{\rho u_1 u_2}|$ quadrupoles are larger than those of $|\widehat{\rho u_2 u_2}|$ by one order of magnitude. These figures allow an assessment of Mach number effects on the spatial distribution of quadrupole sources due to Reynolds stresses.

One can see in Fig. 4 that, for the cylinder vortex shedding frequency, magnitudes of Reynolds stresses are negligible along the airfoil wake region. In the same figure, larger values of $|\widehat{\rho u_1 u_2}|$ are observed along the cylinder wake region for $M_\infty = 0.5$. There is thus a significant compressibility effect on the quadrupole distribution as the Mach number is changed from 0.3 to 0.5.

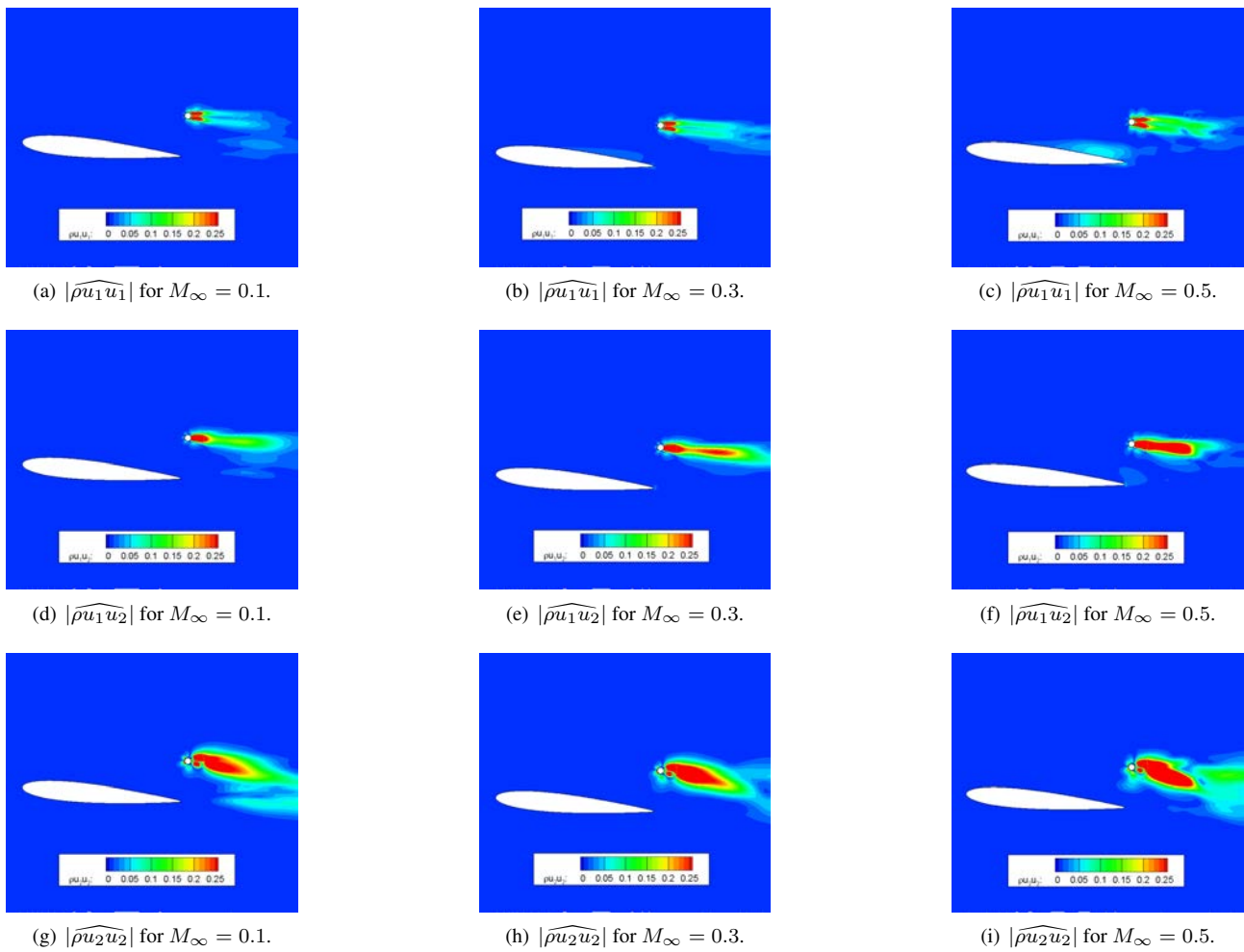


Figure 4. Frequency domain Reynolds stresses normalized by maximum field values for cylinder vortex shedding frequency and cylinder at trailing edge position.

In Fig.5 one can observe results of acoustic predictions for case 5 for the cylinder vortex shedding frequency, which corresponds to $He = 9.5$ and $St = 5.0$. Quadrupole sources have a small contribution to far field radiation.

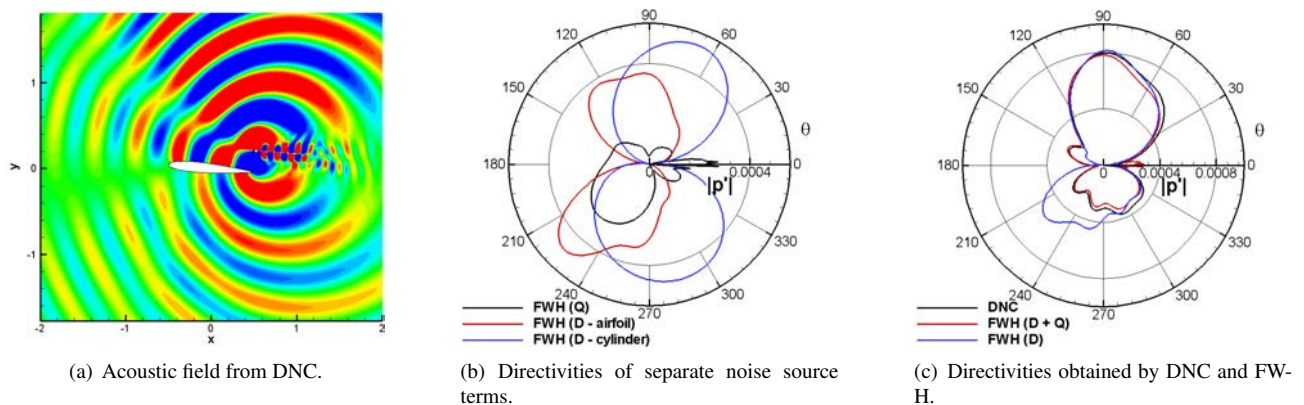


Figure 5. Acoustic predictions for $M_\infty = 0.3$, cylinder at trailing edge position and results at the cylinder vortex shedding frequency.

Figure 6 presents acoustic prediction results of case 6 for the cylinder vortex shedding frequency. Unlike the $M_\infty = 0.3$ case, figure 6 (b) and (c) show that the total noise radiation is obtained by the sum of sound fields from dipole and quadrupole sources, the latter being no longer negligible. In [Wolf et al. \(2012\)](#), the authors demonstrate that quadrupole sources are only relevant for acoustic predictions of moderate Mach number flows at high frequencies. The present results indicate that, even at low frequencies, quadrupole sources are of paramount importance for the total noise prediction of a

moderate Mach number flow with wake interaction.

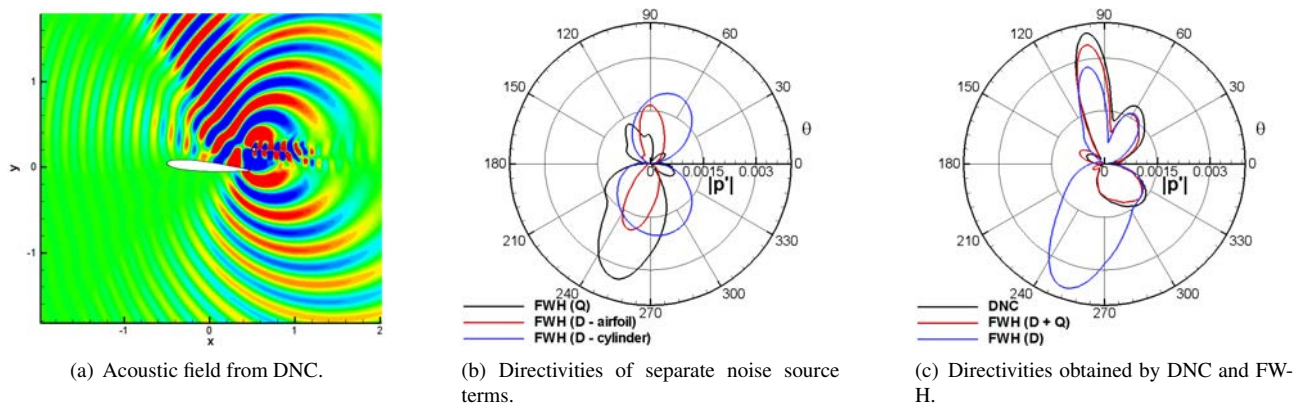


Figure 6. Acoustic predictions for $M_\infty = 0.5$, cylinder at trailing edge position and results at the cylinder vortex shedding frequency.

5. INVESTIGATION OF SOUND-SOURCE MECHANISMS

The results presented in the previous sections showed a significant Mach number dependence of the sound radiation by the studied flow. In order to understand in more detail the role of compressibility, we investigate here the $M = 0.3$ and $M = 0.5$ flows, with the cylinder at the trailing edge position. For the first case, quadrupole radiation is relatively small, whereas for the higher Mach number flow, there is a substantial increase of the contribution of quadrupoles.

5.1 Wave-packet structure of the cylinder wake

We see in figure 7 the amplitude of pressure fluctuations for the cylinder vortex-shedding frequency in the cylinder wake. The amplitude modulation of the fluctuations in the wake, shown in figure 7, and the visualizations of a wavy structure for the pressure fluctuations in figures 5(a) and 6(a) show that fluctuations in the wake can be described as a hydrodynamic wavepacket.

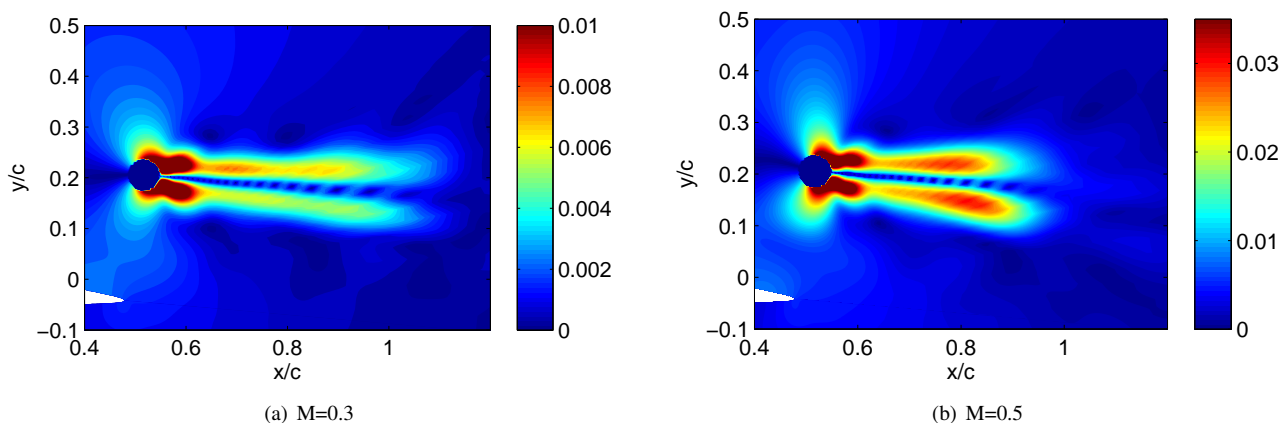


Figure 7. Amplitude of pressure fluctuations for the cylinder vortex shedding frequency.

We note that for $M = 0.3$, the wave-packet amplitudes are low and there is little amplitude growth far from the cylinder. For $M = 0.5$ we note substantially higher amplitudes, and a significant amplitude growth between $x/c = 0.6$ and $x/c = 0.8$.

Another difference is related to the decay of the wavepacket. For the $M = 0.5$ case, there is a sudden decay around $x/c = 0.85$. For the lower Mach number, the decay is smooth, and the wavepacket extends downstream of $x/c = 1$.

In the following section, we will study the linear stability of the cylinder wakes to understand the differences between the two flows analyzed.

5.2 Linear stability analysis of the cylinder wake

5.2.1 Mathematical model and numerical methods

Considering linearised inviscid disturbances in a parallel, sheared flow with velocity profile $U(y)$, and that the pressure fluctuations are given as

$$p'(x, y, t) = p(y) \exp[i(\alpha x - \omega t)] \quad (7)$$

we obtain the Rayleigh equation, which for compressible isothermal flow is given as (Criminale *et al.*, 2003)

$$\frac{d^2 p}{dy^2} - \frac{2U}{U-c} \frac{dp}{dy} - \alpha^2 [1 - M^2(U-c)^2] = 0 \quad (8)$$

where $c = \omega/\alpha$ is the complex-valued phase speed of the instability wave.

When we consider spatially growing or decaying disturbances, the frequency ω is a given real quantity, and the wavenumber $\alpha = \alpha_r + i\alpha_i$ is a complex-valued eigenvalue. The negative of its imaginary part, $-\alpha_i$, is the spatial growth rate of the instability wave.

We solve directly the eigenvalue problem of eq. (8) using a pseudo-spectral method to discretize the derivatives (Trefethen, 2000). Calculations were done with 200 Chebyshev polynomials. We have mapped the infinite domain into $[-1, 1]$ by the change of variables

$$z = \frac{Ly}{\sqrt{1-y^2}} \quad (9)$$

as in Boyd (2001), where $L = 0.5$ was chosen to provide enough points in the two wakes for the DNS configurations.

The velocity profile $U(y)$ downstream of the airfoil and the cylinder is given by an interaction of the respective wakes. This velocity profile was fitted using the function

$$U(y) = 1 - Q_1 \operatorname{sech}((y - y_{c1})/L_1)^2 - Q_2 \operatorname{sech}((y - y_{c2})/L_2)^2. \quad (10)$$

This fit was done for the values of x specified in the next section.

The eigenvalue problem in equation 8 is nonlinear in α . To solve it using standard linear eigenvalue routines, we have transformed it as

$$\begin{bmatrix} 0 & \mathcal{I} & 0 \\ 0 & 0 & \mathcal{I} \\ -\mathcal{F}_0 & -\mathcal{F}_1 & -\mathcal{F}_2 \end{bmatrix} \begin{bmatrix} p \\ \alpha p \\ \alpha^2 p \end{bmatrix} = \alpha \begin{bmatrix} \mathcal{I} & 0 & 0 \\ 0 & \mathcal{I} & 0 \\ 0 & 0 & \mathcal{F}_3 \end{bmatrix} \begin{bmatrix} p \\ \alpha p \\ \alpha^2 p \end{bmatrix} \quad (11)$$

where \mathcal{I} is the identity operator, and \mathcal{F}_i are operators for terms of the equation with order i in α . The \mathcal{F}_i operators are given as

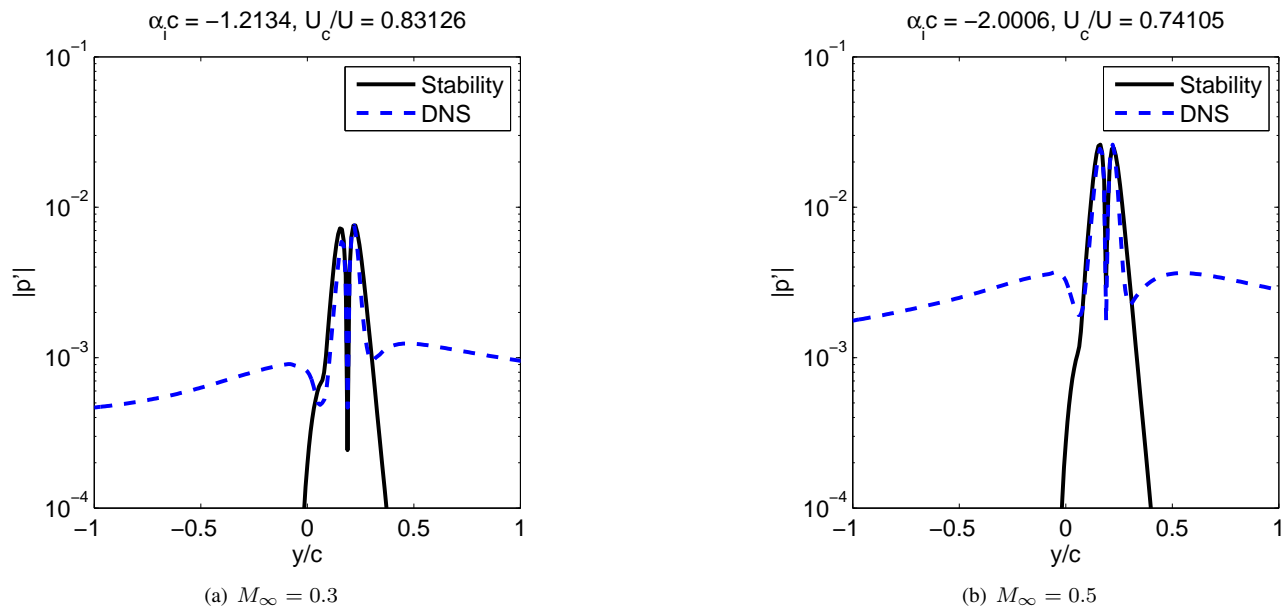
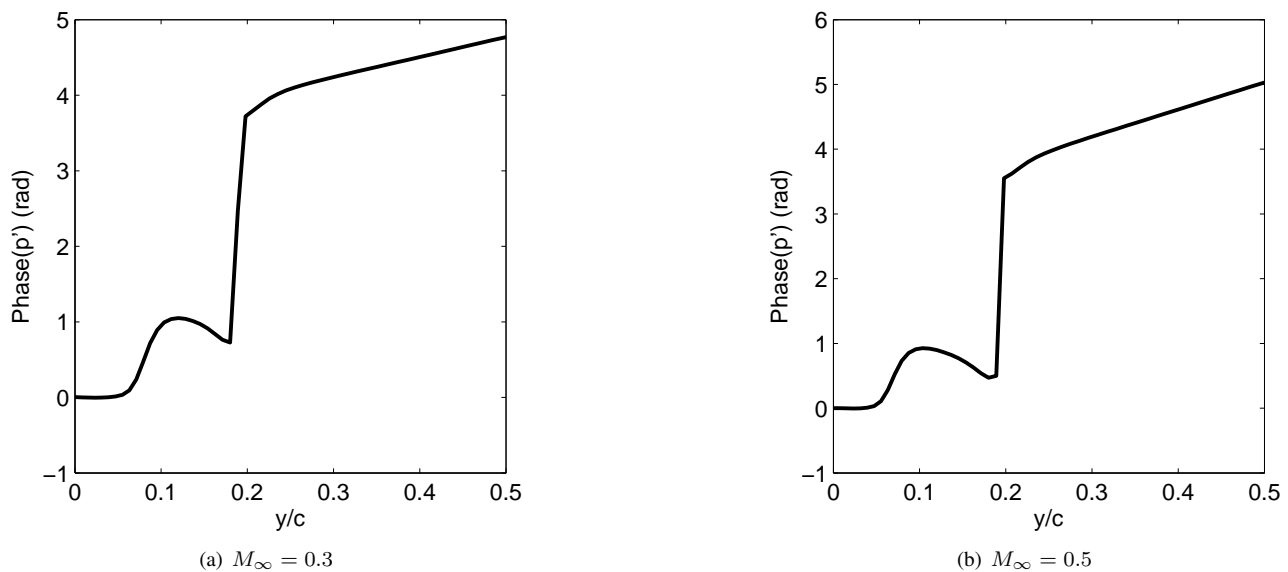
$$\mathcal{F}_3 = -U\mathcal{I} + U^3 M^2 \mathcal{I} \quad (12)$$

$$\mathcal{F}_2 = \omega\mathcal{I} - 3U^2 \omega M^2 \mathcal{I} \quad (13)$$

$$\mathcal{F}_1 = U \frac{d^2}{dy^2} - 2U' \frac{d}{dy} + 3U\omega^2 M^2 \mathcal{I} \quad (14)$$

$$\mathcal{F}_0 = -\omega \frac{d^2}{dy^2} - \omega^2 M^2 \mathcal{I} \quad (15)$$

A similar approach was used and validated in previous work by our group dealing with the linear stability of shear layers (Cavaliere and Agarwal, 2013).

Figure 8. Comparison between DNS and linear stability results at $x/c = 0.7$.Figure 9. Phases of the linear stability eigenfunction at $x/c = 0.7$.

5.2.2 Linear stability results

We compare the most unstable eigenfunction obtained in the stability analysis with the pressure fluctuations in the DNS. Figure 8 shows this comparison at $x/c = 0.7$. The double bump observed in the DNS is accurately reproduced by the linear stability eigenfunction for both Mach numbers. For high $|y|$, the pressure fluctuations in the DNS are acoustic waves, which cannot be obtained using parallel-flow stability calculations.

The cited double bump can be related to the von Kármán vortex street behind the cylinder. Figure 9 shows the phases of the stability eigenfunction. For both Mach numbers, there is a phase jump of approximately π around $y = 0.2$, which corresponds to the center of the wake; this phase opposition between the two sides of the wake is expected for the antisymmetric von Kármán vortex street.

There is a significant compressibility effect in the growth rates for the two cases ($\alpha_i c = -1.2134$ for $M_\infty = 0.3$ and $\alpha_i c = -2.0006$ for $M_\infty = 0.5$). This can be related to the maximum amplitude of the wavepackets in the cylinder wake: recall that for $M_\infty = 0.5$ higher amplifications were seen in figure 7.

Figure 10 shows a similar comparison, this time performed for $x/c = 0.8$. As in the previous position, the linear stability eigenfunction represents accurately the pressure fluctuations in the cylinder wake. However, this time the growth rate for $M_\infty = 0.5$ is lower than that for $M_\infty = 0.3$.

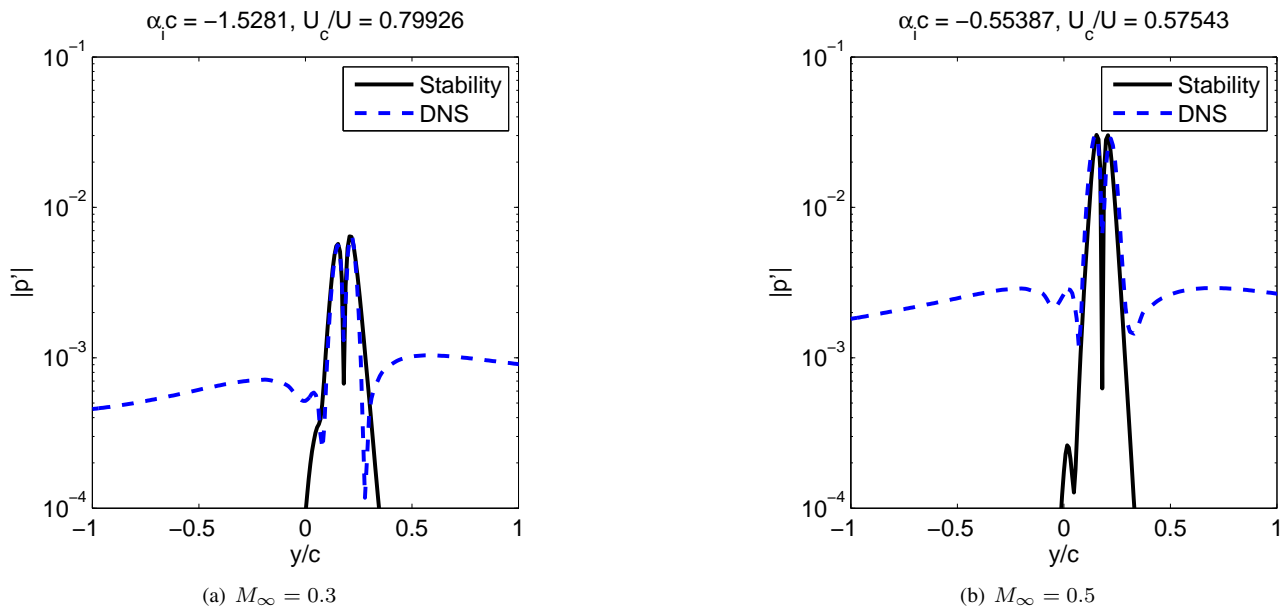


Figure 10. Comparison between DNS and linear stability results at $x/c = 0.8$.

As we move downstream, the $M_\infty = 0.3$ wake continues to present an unstable mode. This was confirmed by the stability analysis at $x/c = 0.9$ and $x/c = 1.0$, shown in figure 11. On the other hand, for the $M_\infty = 0.5$ flow there are only stable modes, which lead to a spatial decay of the wavepacket in this region. This explains the sudden truncation of the $M_\infty = 0.5$ wavepacket and the downstream persistence of the wavepacket for $M_\infty = 0.3$.

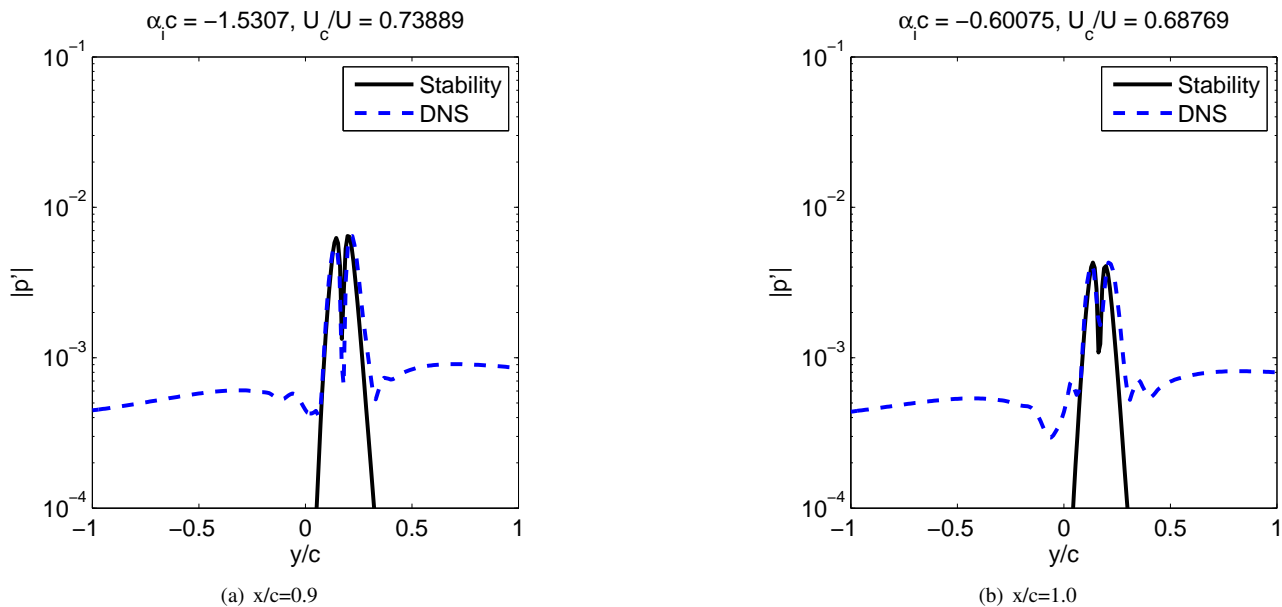


Figure 11. Comparison between DNS and linear stability results for $M_\infty = 0.3$. Similar analysis done for $M_\infty = 0.5$ revealed only stable modes.

5.2.3 Discussion

The agreement between the calculated eigenfunctions and the pressure fluctuations in the DNS shows that linear stability is an appropriate framework to study the fluctuations in the cylinder wake. Based on the results of the previous section, we can cite the following reasons, all of which explain the higher sound emission by the wake at $M_\infty = 0.5$:

1. Near the cylinder, the $M_\infty = 0.5$ wave presents higher spatial amplification, which leads to higher fluctuation amplitudes if compared to the $M = 0.3$ case;

2. As we move downstream, the $M_\infty = 0.5$ wavepacket undergoes a sudden truncation, which is known to result in an increased sound radiation (Cavalieri *et al.*, 2011);
3. For $M_\infty = 0.5$, the convective Mach numbers are higher than in the $M_\infty = 0.3$ case (note that $M_c = (U_c/U)M_\infty$).

6. CONCLUSIONS

In the present work we have studied in detail a numerical simulation of a model airframe noise problem consisting of a two-dimensional configuration composed of a cylinder placed above a NACA 0012 airfoil at 5 deg. angle of incidence. Related work (Wolf *et al.*, 2013) using this simulation has shown that while for $M_\infty = 0.3$ there is little quadrupole radiation, for $M_\infty = 0.5$ the quadrupole distribution in the wake has non-negligible sound radiation. The volume integrals in Ffowcs Williams and Hawkings (1969) cannot thus be neglected even for this moderate Mach number.

These significant differences in the sound radiation by quadrupoles between the $M_\infty = 0.3$ and $M_\infty = 0.5$ flows is studied using a linear stability calculation, which is seen to be pertinent for the present flow due to the close agreement between the stability eigenfunctions and the fluctuations in the cylinder wake. It was seen that, for the higher Mach number, compressibility effects lead to the formation of a wavepacket with higher maximum amplitude, higher convection Mach number and a sudden spatial decay, all of which lead to an increase of quadrupole radiation and explain why quadrupole radiation is much higher for $M_\infty = 0.5$ than for $M_\infty = 0.3$.

ACKNOWLEDGMENTS

The authors acknowledge the financial support received from FAPESP under Grants No. 2011/12493-6 and No. 2013/03508-5.

- Beam, R.M. and Warming, R.F., 1978. "An implicit factored scheme for the compressible navier-stokes equations". *AIAA journal*, Vol. 16, No. 4.
- Bhaskaran, R. and Lele, S.K., 2010. "Large eddy simulation of free-stream turbulence effects on heat transfer to a high-pressure turbine cascade". *Journal of Turbulence*, , No. 11.
- Boyd, J.P., 2001. *Chebyshev and Fourier spectral methods*. Dover publications.
- Cavalieri, A.V.G., Jordan, P., Agarwal, A. and Gervais, Y., 2011. "Jittering wave-packet models for subsonic jet noise". *Journal of Sound and Vibration*, Vol. 330, No. 18-19, pp. 4474–4492. ISSN 1364-503X. doi:10.1016/j.jsv.2011.04.007.
- Cavalieri, A.V.G. and Agarwal, A., 2013. "The effect of base-flow changes in kelvin-helmholtz instability". In *19th AIAA/CEAS Aeroacoustics Conference and Exhibit*. Berlin, Germany.
- Criminale, W.O., Jackson, T.L. and Joslin, R.D., 2003. *Theory and computation of hydrodynamic stability*. Cambridge Univ Pr.
- Ffowcs Williams, J.E. and Hawkings, D.L., 1969. "Sound generation by turbulence and surfaces in arbitrary motion". *Royal Society of London Philosophical Transactions Series A*, Vol. 264, pp. 321–342.
- Jordan, P. and Colonius, T., 2013. "Wave packets and turbulent jet noise". *Annual Review of Fluid Mechanics*, Vol. 45, No. 1.
- Lele, S.K., 1992. "Compact finite difference schemes with spectral-like resolution". *Journal of Computational Physics*, Vol. 103, No. 1, pp. 16–42.
- Lighthill, M.J., 1952. "On sound generated aerodynamically. I. General theory". *Proceedings of the Royal Society of London. Series A, Mathematical and Physical Sciences*, pp. 564–587.
- Nagarajan, S., Lele, S.K. and Ferziger, J.H., 2003. "A robust high-order compact method for large eddy simulation". *Journal of Computational Physics*, Vol. 191, No. 2, pp. 392–419.
- Trefethen, L.N., 2000. *Spectral methods in MATLAB*, Vol. 10. Society for Industrial Mathematics.
- Wang, M., Freund, J.B. and Lele, S.K., 2006. "Computational Prediction of Flow-Generated Sound". *Annual Review of Fluid Mechanics*, Vol. 38, pp. 483–512.
- Wolf, W.R., Azevedo, J.L.F. and Lele, S.K., 2012. "Convective effects and the role of quadrupole sources for aerofoil aeroacoustics". *Journal of Fluid Mechanics*, Vol. 708, p. 502.
- Wolf, W.R. and Lele, S.K., 2010. "Acoustic analogy formulations accelerated by fast multipole method for two-dimensional aeroacoustic problems". *AIAA journal*, Vol. 48, No. 10, pp. 2274–2285.
- Wolf, W.R. and Lele, S.K., 2011. "Aeroacoustic integrals accelerated by fast multipole method". *AIAA journal*, Vol. 49, No. 7, pp. 1466–1477.
- Wolf, W.R., Backes, B., Morsch-Filho, E. and Azevedo, J.L.F., 2013. "Investigation of noise sources in a two-dimensional model airframe noise problem with wake interaction". In *19th AIAA/CEAS Aeroacoustics Conference and Exhibit*. Berlin, Germany.